



This is a repository copy of *Magneto-acoustic Waves in a Magnetic Slab Embedded in an Asymmetric Magnetic Environment: The Effects of Asymmetry*.

White Rose Research Online URL for this paper:
<http://eprints.whiterose.ac.uk/127748/>

Version: Published Version

Article:

Zsamberger, N.K., Allcock, M. orcid.org/0000-0002-0771-743X and Erdelyi, R. (2018) Magneto-acoustic Waves in a Magnetic Slab Embedded in an Asymmetric Magnetic Environment: The Effects of Asymmetry. *Astrophysical Journal*, 853 (2). 136. ISSN 0004-637X

<https://doi.org/10.3847/1538-4357/aa9ffe>

Reuse

This article is distributed under the terms of the Creative Commons Attribution (CC BY) licence. This licence allows you to distribute, remix, tweak, and build upon the work, even commercially, as long as you credit the authors for the original work. More information and the full terms of the licence here:
<https://creativecommons.org/licenses/>

Takedown




If you consider content in White Rose Research Online to be in breach of UK law, please notify us by emailing eprints@whiterose.ac.uk including the URL of the record and the reason for the withdrawal request.



eprints@whiterose.ac.uk
<https://eprints.whiterose.ac.uk/>



Magneto-acoustic Waves in a Magnetic Slab Embedded in an Asymmetric Magnetic Environment: The Effects of Asymmetry

Noémi Kinga Zsámberger^{1,2} , Matthew Allcock¹ , and Róbert Erdélyi^{1,3} ¹ Solar Physics and Space Plasma Research Centre, School of Mathematics and Statistics, University of Sheffield Hicks Building, Hounsfield Road Sheffield, S3 7RH, UK² Department of Physics, University of Debrecen Egyetem tér 1., Debrecen, 4010, Hungary³ Department of Astronomy, Eötvös Loránd University 1/A Pázmány Péter sétány 1117 Budapest, Hungary; robertus@sheffield.ac.uk

Received 2017 October 19; revised 2017 November 30; accepted 2017 December 4; published 2018 January 31

Abstract

Modeling the behavior of magnetohydrodynamic waves in a range of magnetic geometries mimicking solar atmospheric waveguides, from photospheric flux tubes to coronal loops, can offer a valuable contribution to the field of solar magneto-seismology. The present study uses an analytical approach to derive the dispersion relation for magneto-acoustic waves in a magnetic slab of homogeneous plasma enclosed on its two sides by semi-infinite plasma of different densities, temperatures, and magnetic field strengths, providing an asymmetric plasma environment. This is a step further in the generalization of the classic magnetic slab model, which is symmetric about the slab, was developed by Roberts, and is an extension of the work by Allcock & Erdélyi where a magnetic slab is sandwiched in an asymmetric nonmagnetic plasma environment. In contrast to the symmetric case, the dispersion relation governing the asymmetric slab cannot be factorized into separate sausage and kink eigenmodes. The solutions obtained resemble these well-known modes; however, their properties are now mixed. Therefore we call these modes quasi-sausage and quasi-kink modes. If conditions on the two sides of the slab do not differ strongly, then a factorization of the dispersion relation can be achieved for the further analytic study of various limiting cases representing a solar environment. In the current paper, we examine the incompressible limit in detail and demonstrate its possible application to photospheric magnetic bright points. After the introduction of a mechanical analogy, we reveal a relationship between the external plasma and magnetic parameters, which allows for the existence of quasi-symmetric modes.

Key words: magnetohydrodynamics (MHD) – Sun: corona – Sun: magnetic fields – Sun: photosphere – Sun: oscillations – waves

1. Introduction

The solar atmosphere is a dynamic and inhomogeneous medium with plenty of structuring that enables the propagation of a wide range of magnetohydrodynamic (MHD) waves. Two key factors that shape and structure this environment are gravity, which facilitates vertical stratification, and magnetic fields, which are able to sustain structuring both perpendicular and parallel to the field (Roberts 1981b). The ubiquitous magnetic fields and their interaction with the plasma give rise to numerous wave phenomena in both the lower and the upper layers of the atmosphere, turning it into a complex, coupled system (De Pontieu et al. 2005; Komm et al. 2015). A variety of magnetic structures, such as spicules, flares, coronal loops, arcades, and plumes, have been observed that may induce or guide perturbations in the plasma (Aschwanden 2005; Banerjee et al. 2007; de Moortel 2009; Zaqrashvili & Erdélyi 2009; Mathioudakis et al. 2013; Arregui 2015). The physical parameters and the geometric structuring of the medium determine the properties of the supported waves. The detection of wave phenomena and their analysis (ideally inversion, which is often very difficult to achieve in practice) by the means of solar magneto-seismology (SMS), in turn, offer us a tool to deduce unknown properties of the plasma (Andries et al. 2009; Ruderman & Erdélyi 2009; Morton et al. 2012).

On the theoretical side, the assumption that there are MHD waves in the solar atmosphere, especially in the corona, was made decades ago (Uchida 1968; Habbal et al. 1979; Roberts 1981b). Observationally, the existence of slow magneto-acoustic waves in coronal loops has been deduced based on modulated radio emission; furthermore, several oscillations have been detected in prominences and in the proximity of sunspots, which are well interpreted in terms of MHD wave phenomena (Roberts 2000; Wang 2011; Arregui et al. 2012). However, the majority of the research on MHD waves remained theoretical, due to the limited number of available observations. In this respect, a fundamental change has transpired in the past few decades, as both photographic and spectroscopic instruments have achieved higher spatial and temporal resolution. The 1998 detection of transversal (fast magneto-acoustic) waves in coronal loops with the help of *Transition Region and Coronal Explorer (TRACE)* has become a symbol of this scientific turning point (Aschwanden et al. 1999; Ruderman & Erdélyi 2009; De Moortel & Nakariakov 2012).

Theoretical and practical interest in MHD waves is motivated by fundamental questions of solar physics, namely understanding the physical processes contributing to the heating of the solar atmosphere and diagnosing the highly structured and stratified atmosphere. Of course, these two tasks are interwoven, as the heating process(es) likely depend on the local plasma equilibrium (De Moortel & Browning 2015). In brief on theoretical developments, Roberts was among the first ones to suggest the utilization of SMS in the coronal context



Original content from this work may be used under the terms of the [Creative Commons Attribution 3.0 licence](https://creativecommons.org/licenses/by/3.0/). Any further distribution of this work must maintain attribution to the author(s) and the title of the work, journal citation and DOI.

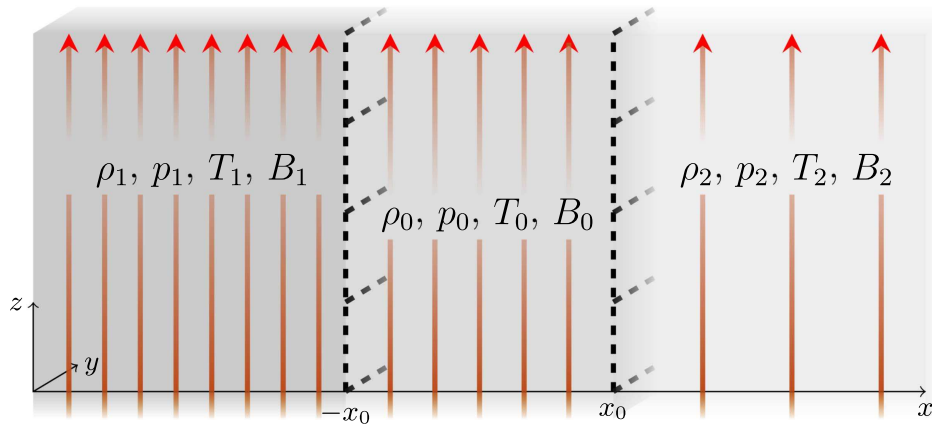


Figure 1. Equilibrium conditions: inside the slab, $|x| \leq x_0$ (medium gray), and outside the slab, $x < -x_0$ and $x > x_0$ (light and dark gray). The red arrows illustrate the vertical magnetic fields, $B_0 \hat{z}$, $B_1 \hat{z}$, and $B_2 \hat{z}$; the dashed black lines outline the boundaries of the slab.

(Roberts 1981b; Arregui 2015). In a series of studies, Roberts (1981a, 1981b) and Edwin & Roberts (1982) examined the propagation of linear magneto-acoustic waves in structured magnetic fields (ignoring the effects of gravity) in an inviscid ideal plasma. First, a single interface was considered, which separated two regions of different density and magnetic field strength. A discontinuity, one side of which is field-free, was found to give rise to a slow magneto-acoustic surface mode, and when the magnetic plasma was cooler than the adjacent medium, a fast surface mode (Roberts 1981b). This research was expounded upon by introducing not one, but two surfaces of discontinuity, that is by examining wave propagation along a symmetric magnetic slab in a nonmagnetic environment. It was determined that both so-called surface and body waves may be supported in the slab geometry. This nomenclature reflects whether the waves are evanescent or have nodes of increased perturbation inside the slab. Recall, for trapped waves, that it is always assumed that the waves are evanescent outside the waveguide. This assumption is held throughout this paper as well. The existence and nature of the waves in a certain case, however, depends upon the ordering of the characteristic speeds inside the slab and in its environment (Roberts 1981a).

The magnetic slab model was further generalized by Allcock & Erdélyi (2017), who investigated the emerging wave physics that arise from setting different thermodynamic equilibrium conditions for the two sides of the slab; that is, the external nonmagnetic medium is asymmetric. In their work, the examination of the different modes was complemented by a parametric analysis into the effect that changing the ratio of the external densities has on the dispersion of the waves. A key point of the introduced asymmetry is that the modes are modified from the traditional sausage and kink modes, as the amplitudes across the slab are affected by the different external media at the slab boundaries (Allcock & Erdélyi 2017).

Edwin & Roberts (1982) investigated the propagation of magneto-acoustic waves along a magnetic slab in a symmetric magnetic environment. The aim of the present work is to build upon and to generalize further their symmetric slab model. To achieve this, we introduce asymmetry into the model, thus place the slab in an asymmetric magnetic environment by allowing the magnetic field strength, density, and temperature in the external plasma to be distinct on each side of the slab.

First, we derive the general dispersion relation, then validate the results with those of Edwin & Roberts (1982) for the symmetric environment and Allcock & Erdélyi (2017) for the

asymmetric but field-free environment in Section 2. In Section 3, we present the limit of incompressible plasma as an interesting specific case of the asymmetric slab problem, which may be an appropriate approximation of MHD wave propagation in magnetic bright points (MBPs). Last, in Section 4, we propose a mechanical analogy for the asymmetric slab system and derive a condition for the external parameters that enables the existence of quasi-symmetric oscillations with a given frequency and wavenumber.

2. Derivation of the Dispersion Relation

The current examination pertains to a 3D, inviscid, static, ideal plasma under an equilibrium magnetic field, $B_0(x) \hat{z}$, where \hat{z} is the unit vector in the vertical direction. Gravity is ignored. The volume is divided into three regions of different magnetic field strength:

$$B_0(x) = \begin{cases} B_1, & x < -x_0, \\ B_0, & |x| < x_0, \\ B_2, & x > x_0, \end{cases} \quad (1)$$

where B_0 , B_1 , and B_2 are constants. Furthermore, the plasma is uniform within each region with different equilibrium plasma pressure (p_i), density (ρ_i), and temperature (T_i). Quantities describing the inside of the slab are denoted by the subscript $i = 0$, while quantities outside the slab carry the subscripts $i = 1, 2$, as shown by Figure 1. Only the effects of density and magnetic perturbations are considered, while those of gravity or background bulk motions are not considered within the scope of this study.

The stability of the equilibrium conditions requires equilibrium total pressure balance across each interface. This demands that the total (gas plus magnetic) pressure is constant:

$$p_1 + \frac{B_1^2}{2\mu} = p_0 + \frac{B_0^2}{2\mu} = p_2 + \frac{B_2^2}{2\mu}, \quad (2)$$

where μ is the permeability of free space. The sound speed in each region can be expressed as $c_i = \sqrt{\gamma p_i / \rho_i}$ for $i = 0, 1, 2$. Here, γ is the adiabatic index, which is uniform across every domain, under the assumption that the plasma composition in the entire volume is the same. Another characteristic speed in the plasma, i.e., the Alfvén speed, is denoted by $v_{Ai} = B_i / \sqrt{\rho_i \mu}$ for $i = 0, 1, 2$. Equation (2), which describes the equilibrium

pressure balance, yields the following relationship between the density ratios and characteristic speeds for any two regions:

$$\frac{\rho_i}{\rho_j} = \frac{c_j^2 + \frac{1}{2}\gamma v_{Aj}^2}{c_i^2 + \frac{1}{2}\gamma v_{Ai}^2}, \quad \text{where } i = 0, 1, 2; \\ j = 0, 1, 2; \quad i \neq j. \quad (3)$$

Disturbances within the slab, as well as in its magnetic environment, are governed by the ideal MHD equations:

$$\frac{\partial \rho}{\partial t} + \nabla \cdot (\rho \mathbf{v}) = 0 \quad (4)$$

$$\rho \frac{D\mathbf{v}}{Dt} = -\nabla p - \frac{1}{\mu} \mathbf{B} \times (\nabla \times \mathbf{B}) \quad (5)$$

$$\frac{\partial \mathbf{B}}{\partial t} = \nabla \times (\mathbf{v} \times \mathbf{B}) \quad (6)$$

$$\frac{D}{Dt} \left(\frac{p}{\rho^\gamma} \right) = 0, \quad (7)$$

where $\mathbf{v} = (v_x, v_y, v_z)$, \mathbf{B} , p , and ρ are the velocity, magnetic field strength, pressure, and density, respectively. Equation (4) expresses mass conservation, Equations (5) and (6) are the momentum and induction equations, respectively, and Equation (7) is the energy equation for adiabatic processes. We linearize these equations about a static basic state and seek plane-wave solutions propagating in the \hat{z} direction of the form

$$v_x(\mathbf{x}, t) = \hat{v}_x(x) e^{i(kz - \omega t)}, \\ v_y(\mathbf{x}, t) = 0, \\ v_z(\mathbf{x}, t) = \hat{v}_z(x) e^{i(kz - \omega t)}, \quad (8)$$

where k is the z component of the wavenumber vector defined as $\mathbf{k} = (0, 0, k)$, and ω is the angular frequency.

The linearized governing equations then reduce to a single ordinary differential equation for each region, which governs perturbations in that region, given by

$$\hat{v}_x'' - m_j^2 \hat{v}_x = 0, \quad (9)$$

where

$$m_j^2 = \frac{(k^2 v_{Aj}^2 - \omega^2)(k^2 c_j^2 - \omega^2)}{(v_{Aj}^2 + c_j^2)(k^2 c_{Tj}^2 - \omega^2)}, \quad j = 0, 1, 2, \quad (10)$$

are wavenumber coefficients and

$$c_{Tj}^2 = \frac{v_{Aj}^2 c_j^2}{v_{Aj}^2 + c_j^2} \quad (11)$$

are the tube speeds for each domain for $j = 0, 1, 2$.

The solutions to Equation (9) are a linear combination of the hyperbolic functions. Physically realistic solutions prescribe that the slab perturbations have no effect on plasma far away from the system; that is, the waves are evanescent outside the slab. This imposes the restriction on \hat{v}_x that as $x \rightarrow \pm\infty$, $\hat{v}_x \rightarrow 0$, and so $m_1^2 > 0$ and $m_2^2 > 0$. The general solution in this case takes the form

$$\hat{v}_x(x) = \begin{cases} A(\cosh m_1 x + \sinh m_1 x), & x < -x_0, \\ B \cosh m_0 x + C \sinh m_0 x, & |x| < x_0, \\ D(\cosh m_2 x - \sinh m_2 x), & x_0 < x. \end{cases} \quad (12)$$

Here, A , B , C , and D are arbitrary real constants. Physical solutions further require that two boundary conditions be fulfilled: the perturbations in velocity have to be continuous, and total pressure balance has to be upheld across the slab boundaries at $x = \pm x_0$. Applying these boundary conditions gives us four homogeneous algebraic equations in terms of the constants A , B , C , and D . Nontrivial solutions only exist when the determinant of the coefficients of this system of equations is zero. This gives us the dispersion relation as

$$2(\Lambda_0^2 + \Lambda_1 \Lambda_2) + \Lambda_0(\Lambda_1 + \Lambda_2) \left[\tau_0 + \frac{1}{\tau_0} \right] = 0, \quad (13)$$

where

$$\tau_0 = \tanh m_0 x_0, \quad (14)$$

$$\Lambda_j = -\frac{i \rho_j k^2 v_{Aj}^2 - \omega^2}{\omega m_j}, \quad j = 0, 1, 2. \quad (15)$$

By substituting Λ_j for $j = 0, 1, 2$ into Equation (13), we can express the dispersion relation in terms of wavenumbers, frequencies, and characteristic speeds as

$$2m_0^2(k^2 v_{A1}^2 - \omega^2)(k^2 v_{A2}^2 - \omega^2) + 2\frac{\rho_0}{\rho_1} m_1 \frac{\rho_0}{\rho_2} m_2 (k^2 v_{A0}^2 - \omega^2)^2 \\ + \rho_0 m_0 (k^2 v_{A0}^2 - \omega^2) \left[\frac{m_2}{\rho_2} (k^2 v_{A1}^2 - \omega^2) + \frac{m_1}{\rho_1} (k^2 v_{A2}^2 - \omega^2) \right] \\ \times \left[\tau_0 + \frac{1}{\tau_0} \right] = 0. \quad (16)$$

2.1. Validation with Earlier Studies

There are at least two earlier models that the current results should remain consistent with. If we set $B_1 = B_2 = 0$, thus $v_{A1} = v_{A2} = 0$, then the wavenumbers m_1 and m_2 revert back to

$$m_j^2 = \frac{(k^2 c_j^2 - \omega^2)}{c_j^2}, \quad \text{for } j = 1, 2. \quad (17)$$

Furthermore, the dispersion relation (Equation (16)) loses the factors containing the external Alfvén speeds and simplifies to

$$\omega^4 m_0^2 + \frac{\rho_0}{\rho_1} m_1 \frac{\rho_0}{\rho_2} m_2 (k^2 v_{A0}^2 - \omega^2)^2 - \frac{1}{2} m_0 \omega^2 (k^2 v_{A0}^2 - \omega^2) \\ \times \left(\frac{\rho_0}{\rho_1} m_1 + \frac{\rho_0}{\rho_2} m_2 \right) \left[\tau_0 + \frac{1}{\tau_0} \right] = 0, \quad (18)$$

which corroborates with the result for the magnetic slab embedded in a nonmagnetic asymmetric environment (Allcock & Erdélyi 2017).

The second way to approach the current model is to build it based on the magnetic slab in a symmetric magnetic environment. The dispersion relation for that case is

$$\rho_e (k^2 v_{Ae}^2 - \omega^2) m_0 \left(\frac{\tanh}{\coth} \right) \{ m_0 x_0 \} + \rho_0 (k^2 v_{A0}^2 - \omega^2) m_e = 0, \quad (19)$$

where external parameters are indexed by e , since they are now the same on either side of the slab (Edwin & Roberts 1982). This, however, gives two decoupled equations: one for the sausage (tanh version) and one for the kink modes (coth), whereas for the general case of the asymmetric slab in a magnetic environment, the dispersion relation does not decouple.

If the densities, pressures, and magnetic fields on the two sides of the slab are of the same order ($\rho_1 \approx \rho_2$, $p_1 \approx p_2$, $B_1 \approx B_2$), and Λ_2 is of the same order as Λ_1 , then the dispersion relation, Equation (16), decouples and approximates to

$$(k^2 v_{A0}^2 - \omega^2) \left[\frac{\rho_0 m_1}{\rho_1 (k^2 v_{A1}^2 - \omega^2)} + \frac{\rho_0 m_2}{\rho_2 (k^2 v_{A2}^2 - \omega^2)} \right] + 2m_0 \left(\frac{\tanh}{\coth} \right) \{m_0 x_0\} = 0. \quad (20)$$

This gives us a separate equation for sausage and kink eigenmodes, which is analogous to the symmetric case. Further, if $\rho_1 = \rho_2 = \rho_e$, $p_1 = p_2 = p_e$, $B_1 = B_2 = B_e$, then Equation (20) reduces to Equation (19), which is the dispersion relation for the slab in a symmetric magnetic environment. In the following section, the consequences of this factorization of the dispersion relation will be discussed.

2.2. Eigenmodes of the Slab in an Asymmetric Magnetic Environment

Whether there is an external magnetic field, or there is none, in the symmetric slab system, the full and exact dispersion relation (Equation (19)) consists of two separate equations without an approximation. The equation containing the odd function $\tanh(m_0 x_0)$ describes the sausage mode, where the velocity perturbation amplitude \hat{v}_x is therefore an odd function; the two boundaries of the slab oscillate in anti-phase. The equation containing the $\coth(m_0 x_0)$ function represents the kink waves, where \hat{v}_x is an even function, thus the oscillation at the slab boundaries is in-phase (Roberts 1981a).

In general, the exact dispersion relation for the asymmetric slab system cannot now be decoupled into an equation governing sausage or kink modes, respectively, neither when there is no magnetic field outside the slab (Allcock & Erdélyi 2017), nor when it is embedded in a magnetic environment (Equation (20)). Both ‘‘sausage’’ and ‘‘kink’’ mode solutions are modified by the differences in external parameters (density, pressure, and magnetic field strength), which manifests, for example, in an asymmetry of the oscillation amplitude on the two sides of the slab (see Figure 2 as a schematic visualization). Therefore, to be as close as possible to the notion introduced by Roberts (1981a), we label the obtained modes of waves of an asymmetric slab geometry as quasi-sausage and quasi-kink.

A special characteristic of (quasi-)sausage modes remains, which is that they possess an unperturbed magnetic surface somewhere in the examined central domain. In the case of a symmetric slab (Roberts 1981a; Edwin & Roberts 1982), this surface is in the center of the slab for the sausage modes. In an asymmetric system with no external magnetic field, the position of this surface is shifted toward the side where the transverse displacement perturbation is smallest. For a slab in a nonmagnetic environment, this is the side bounded by the region of greater external density (Allcock & Erdélyi 2017). If

the asymmetric slab is embedded in an asymmetric magnetic environment, such as in Figure 1, then the position of minimum perturbation is shifted toward the side with higher density and weaker magnetic field strength. Kink modes are not left unchanged by the difference in external parameters, either. The kink waves in a symmetric slab leave the slab’s cross-sectional width unchanged, while the same cannot hold true for the asymmetric system.

The introduction of the asymmetries in the externally magnetized environment will also result in a change of behavior of the surface and body modes. The wave power of surface modes across the slab will have a single minimum. It is located in the center of a symmetric slab, but the inclusion of asymmetry in the externally magnetized plasma will displace it toward one side. The intensity of the maximum amplitudes on the slab boundaries will also be changed to reflect the influence of the disparity between the external plasma parameters. The wave power of body modes is spatially oscillatory instead of evanescent within the slab. The effect of equilibrium plasma and magnetic asymmetry on these waves is that the nodes and anti-nodes of these oscillations are shifted toward one side of the slab. The panels of Figure 3 illustrate the behavior of surface and body modes in a magnetized asymmetric slab system using numerical solutions we found for the dispersion relation (Equation (16)).

3. Analytical Investigation

This section deals with the analytical examination of the dispersion relation derived for the magnetic slab embedded in an asymmetric magnetic environment. Let us now focus on the case of the incompressible limit. Given the complex nature of Equation (13), we demonstrate the derivation of supported waves’ properties based on both the complete (Equation (13)), and the decoupled dispersion relation (Equation (20)). It should be kept in mind that in the latter case, the results included in the section are valid only for such configurations in which the external equilibrium parameters on either side of the slab are of the same order.

With the exception of the spurious solutions brought in through the derivation process, any combination of wave properties that satisfy the dispersion relation describe a wave supported by the slab. Cases when the phase speed of waves corresponds to one of the characteristic speeds in the slab, require separate treatment. We do not investigate the case $\omega^2 = k^2 v_{A0}^2$ in detail, since it would give rise to the Alfvén resonance (for more details see Goossens et al. 2011). However, since we do not consider propagation in the y direction, the Alfvén waves (that would be described by v_y and B_y) become decoupled from the system. On the other hand, when $\omega^2 = k^2 c_{T0}^2$, the governing Equation (9), becomes singular, the ideal MHD equations break, and dissipations should be considered. Both of these possibilities would correspond to resonances for a driven problem, in particular, if the slabs would be nonuniform, resulting in resonant absorption. However, that would be an entirely different study beyond the scope of the current paper.

3.1. The Incompressible Limit

The assumption that the plasma in our system is incompressible simplifies the equations describing wave dispersion. It allows us to focus on effects other than the compressibility and

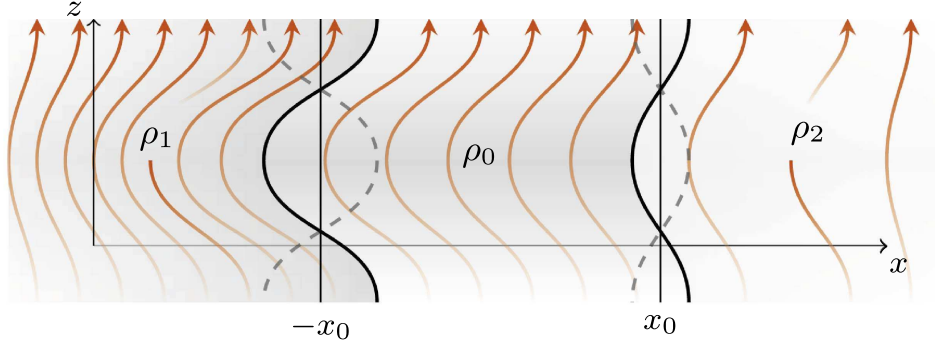
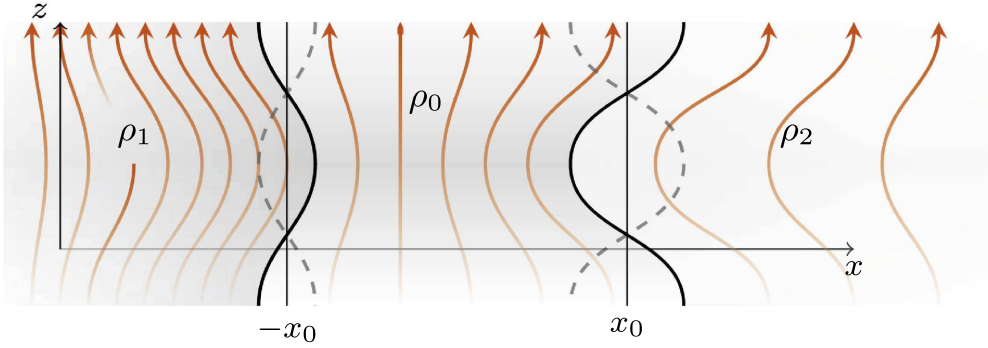

 (a) Illustration of a quasi-kink mode with $\rho_1 > \rho_2$ and $B_1 > B_2$.

 (b) Illustration of a quasi-sausage mode with $\rho_1 > \rho_2$ and $B_1 > B_2$.

Figure 2. Illustration of eigenmodes along a slab in an asymmetric magnetic environment. The red arrows illustrate the perturbed magnetic fields, the thick solid black lines denote the perturbed slab boundaries, and the dashed gray lines indicate the position of the slab boundaries after half of a period.

provide analytical solutions to the dispersion relation. In the limiting case of an incompressible plasma, the sound speeds tend to infinity and $c_T^2 \rightarrow v_A^2$, therefore $m_i \rightarrow k$ for $i = 0, 1, 2$. The decoupled dispersion relation (20) reduces to

$$\begin{aligned} & \left[2 \left(\frac{\tanh}{\coth} \right) \{kx_0\} + \frac{2}{R} \right] \omega^4 - k^2 \left[2(v_{A1}^2 + v_{A2}^2) \left(\frac{\tanh}{\coth} \right) \{kx_0\} \right. \\ & \left. + \frac{\rho_0}{\rho_2} (v_{A0}^2 + v_{A1}^2) + \frac{\rho_0}{\rho_1} (v_{A0}^2 + v_{A2}^2) \right] \omega^2 \\ & + k^4 \left[2v_{A1}^2 v_{A2}^2 \left(\frac{\tanh}{\coth} \right) \{kx_0\} + \frac{\rho_0}{\rho_2} (v_{A0}^2 v_{A1}^2) + \frac{\rho_0}{\rho_1} (v_{A0}^2 v_{A2}^2) \right] \\ & = 0, \end{aligned} \quad (21)$$

which is a quadratic equation for ω^2 . Here, R is the measure of the density asymmetry, defined as

$$R = \left[\frac{\rho_0}{2} \left(\frac{1}{\rho_1} + \frac{1}{\rho_2} \right) \right]^{-1}. \quad (22)$$

If $\rho_1 = \rho_2 = \rho_e$, then R reduces to the ratio of the external to internal densities. The solutions of the above equation are

$$\omega^2 = \frac{-\mathcal{B} \pm \sqrt{\mathcal{B}^2 - 4\mathcal{A}\mathcal{C}}}{2\mathcal{A}}, \quad (23)$$

where

$$\mathcal{A} = \left[2 \left(\frac{\tanh}{\coth} \right) \{kx_0\} + \frac{2}{R} \right], \quad (24)$$

$$\begin{aligned} \mathcal{B} = & -k^2 \left[2(v_{A1}^2 + v_{A2}^2) \left(\frac{\tanh}{\coth} \right) \{kx_0\} + \frac{\rho_0}{\rho_2} (v_{A0}^2 + v_{A1}^2) \right. \\ & \left. + \frac{\rho_0}{\rho_1} (v_{A0}^2 + v_{A2}^2) \right], \end{aligned} \quad (25)$$

$$\mathcal{C} = k^4 \left[2v_{A1}^2 v_{A2}^2 \left(\frac{\tanh}{\coth} \right) \{kx_0\} + \frac{\rho_0}{\rho_2} v_{A0}^2 v_{A1}^2 + \frac{\rho_0}{\rho_1} v_{A0}^2 v_{A2}^2 \right]. \quad (26)$$

If we impose a certain symmetry on the system, namely the external densities are equal $\rho_1 = \rho_2 = \rho_e$, while the external magnetic fields still differ from one another, and introduce the notation

$$\mathcal{T} = \left(\frac{\tanh}{\coth} \right) \{kx_0\}, \quad (27)$$

$$\bar{R} = \frac{\rho_0}{\rho_e}, \quad (28)$$

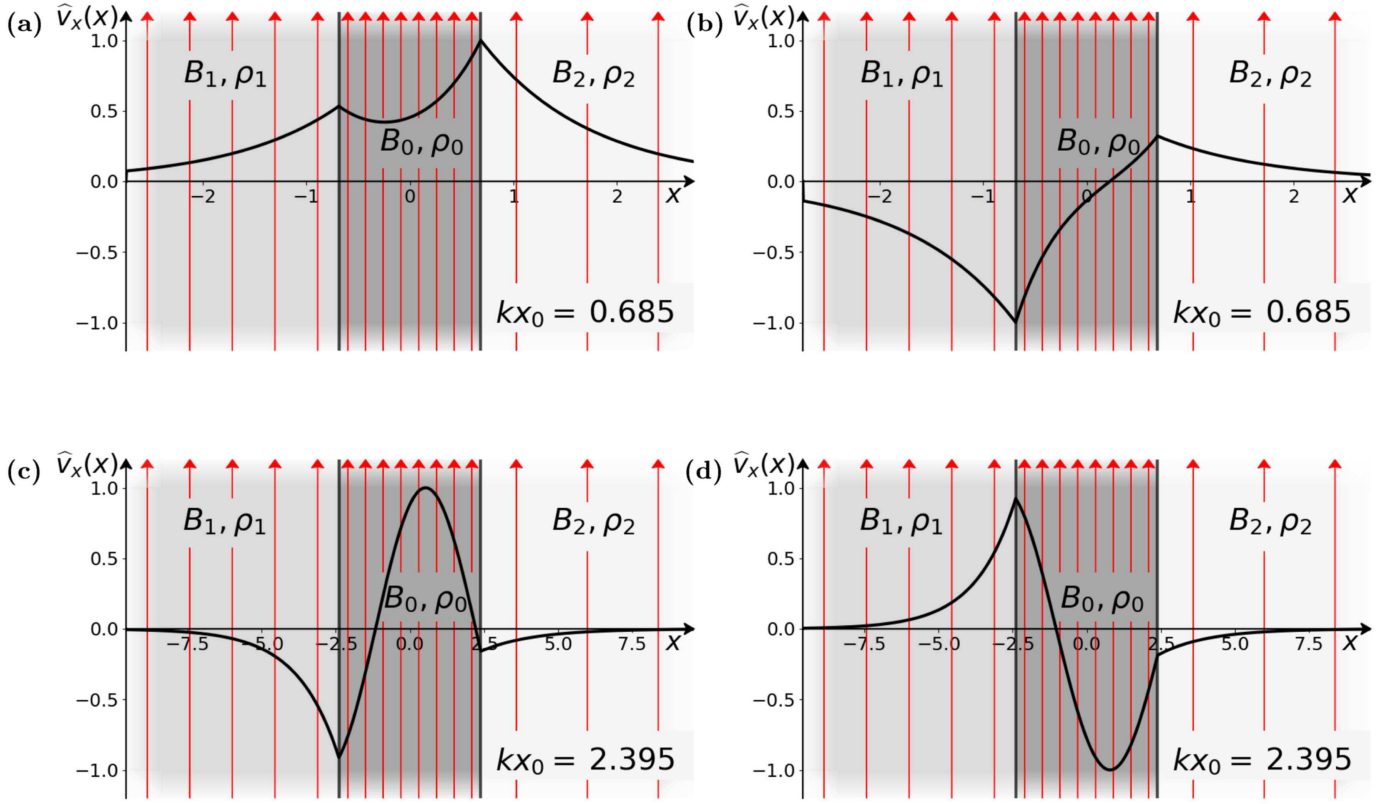


Figure 3. Distribution of the transverse velocity perturbation ($\hat{v}_x(x)$) as a function of the transverse spatial coordinate, x , in a strongly magnetized, dense slab and its rarefied, weaker magnetic asymmetric environment. The red arrows represent the equilibrium magnetic fields, and darker gray shading corresponds to higher background densities. The solid black curves show the amplitude of the transverse velocity perturbation for (a) a slow quasi-sausage surface mode, (b) a slow quasi-kink surface mode, (c) a fast quasi-sausage body mode of order one, and (d) a fast quasi-kink body mode of order one. For panels (a) and (b), the values $v_{A0} = 0.7c_0$, $v_{A1} = 0.2c_0$, $v_{A2} = 0.1c_0$, $c_1 = 2.2279c_0$, $c_2 = 1.8742c_0$, $\rho_1/\rho_0 = 0.28$, and $\rho_2/\rho_0 = 0.4$ were used for solving the dispersion relation, and the eigenmodes of a thin slab ($kx_0 = 0.685$) were visualized. In panels (c) and (d), the body mode solutions of a wider slab ($kx_0 = 2.395$) with the same characteristic speeds and density ratios are displayed.

then the dispersion relation may be written as

$$\begin{aligned} \omega^2 = & \frac{k^2}{2} \frac{1}{\mathcal{T} + \bar{R}} \{ 2[v_{A1}^2 + v_{A2}^2] \mathcal{T} + \bar{R} [2v_{A0}^2 + v_{A1}^2 + v_{A2}^2] \\ & \pm 4[\mathcal{T}^2(v_{A1}^2 - v_{A2}^2)^2 + 4\bar{R}\mathcal{T}(v_{A1}^2 - v_{A2}^2)^2 \\ & + \bar{R}^2(\{2v_{A0}^2 - v_{A1}^2\}^2 + \{2v_{A0}^2 - v_{A2}^2\}^2 - 4v_{A0}^2)]^{1/2} \}. \end{aligned} \quad (29)$$

On the other hand, if the densities are allowed to vary, and the external Alfvén speeds are the same ($v_{A1}^2 = v_{A2}^2 = v_{Ae}^2$), and introduce the notation

$$\mathcal{D} = \frac{\rho_1 + \rho_2}{\rho_0}, \quad (30)$$

$$\mathcal{E} = \frac{\rho_1 \rho_2}{\rho_0^2}, \quad (31)$$

then the dispersion relation may be written as

$$\begin{aligned} \omega^2 = & \frac{k^2}{8} \frac{1}{\mathcal{E}\mathcal{T} + 2\mathcal{E}^2\mathcal{D}\rho_0^2} \left\{ 4\mathcal{E}v_{Ae}^2\mathcal{T} + \frac{\mathcal{D}}{\rho_0}v_{A0}^2 + 2\mathcal{D}v_{Ae}^2 \right. \\ & \pm [\mathcal{D}^2v_{A0}^4 + \mathcal{D}^2v_{Ae}^4 - 2\mathcal{E}v_{Ae}^4 + 8\mathcal{T}\mathcal{D}\mathcal{E}v_{A0}^2v_{Ae}^2 + 8\mathcal{T}\mathcal{D}\mathcal{E}v_{Ae}^4 \\ & + 2\mathcal{D}v_{A0}^2v_{Ae}^2 + 2\frac{\mathcal{E}}{\rho_0}v_{Ae}^4 - 8\mathcal{T}\mathcal{D}\mathcal{E}\rho_0v_{A0}^2v_{Ae}^2 \\ & \left. - 32\mathcal{D}\mathcal{E}^3\rho_0^2v_{Ae}^4\mathcal{T} - 8\mathcal{D}^2\mathcal{E}^2v_{A0}^2v_{Ae}^2]^{1/2} \right\}. \end{aligned} \quad (32)$$

In the case when the magnetic field strength (thus the Alfvén speed) is zero on both sides of the slab, the dispersion relation takes the following concise form:

$$\omega^2 = \frac{k^2}{8} \frac{1}{\mathcal{E}\mathcal{T} + 2\mathcal{E}^2\mathcal{D}\rho_0^2} \left\{ \frac{\mathcal{D}}{\rho_0}v_{A0}^2 \pm \mathcal{D}v_{A0}^2 \right\}. \quad (33)$$

In the incompressible limit, even solutions to the full dispersion relation (Equation (16)) can be expressed in a relatively simple manner:

$$\begin{aligned} \omega^2 = & \frac{k^2}{2\zeta + 4} \{ v_{A0}^2\zeta + \theta + 2(v_{A1}^2 + v_{A2}^2) \pm [v_{A0}^4\zeta^2 + \theta^2 \\ & + (4 + 4v_{A0}^2 + 4\theta)(v_{A1}^2 + v_{A2}^2) - (2\zeta\theta + 8\theta)v_{A0}^2]^{1/2} \}, \end{aligned} \quad (34)$$

where

$$\zeta = \left(\frac{\rho_0}{\rho_1} + \frac{\rho_0}{\rho_2} \right) \left(\tau_0 + \frac{1}{\tau_0} \right) + \frac{2\rho_0^2}{\rho_1\rho_2}, \quad (35)$$

$$\theta = \left(\frac{\rho_0}{\rho_1}v_{A2}^2 + \frac{\rho_0}{\rho_2}v_{A1}^2 \right) \left(\tau_0 + \frac{1}{\tau_0} \right) + \frac{2\rho_0^2}{\rho_1\rho_2}v_{A0}^2, \quad (36)$$

$$\tau_0 = \tanh(kx_0). \quad (37)$$

Parametric examinations (see Figure 4) show that, just as in the case of a field-free environment, the incompressible modes of the asymmetric slab in a magnetic environment tend toward

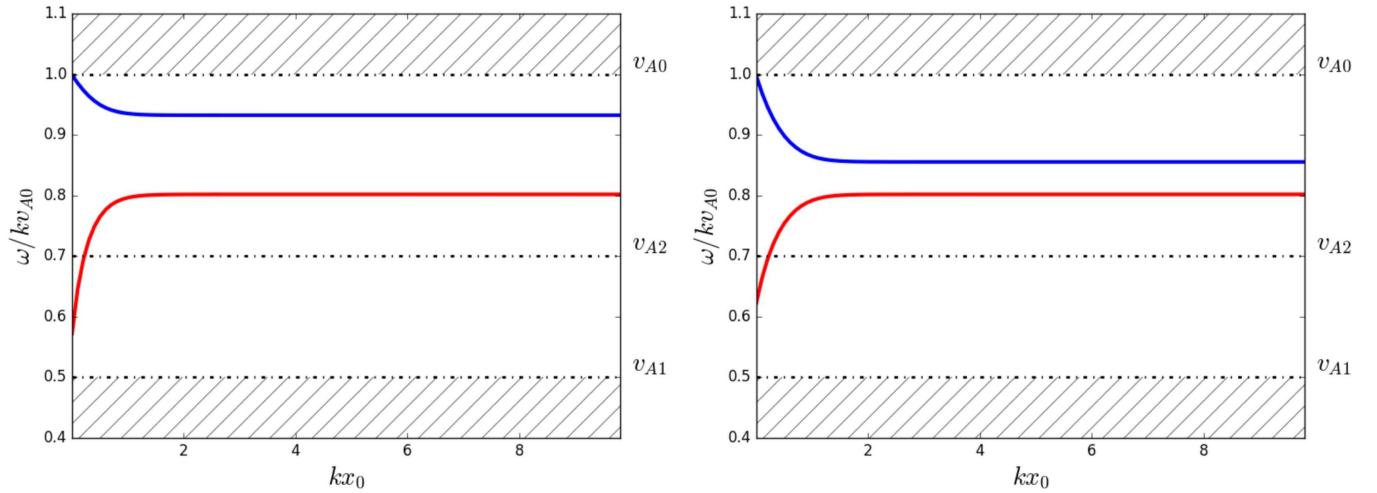


Figure 4. Solution of Equation (23) for $R = 0.5$ (left panel) and $R = 1.0$ (right panel), showing the behavior of magneto-acoustic waves in the limiting case of an incompressible plasma. The blue line indicates the quasi-sausage mode, while the red line shows the quasi-kink mode. The hatching denotes regions in which no modes occur. For the left panel $c_0 \approx 105$, $c_1 = 100$, $c_2 \approx 62$, $v_{A0} = 1.0$, $v_{A1} = 0.5$, $v_{A2} = 0.7$, $\rho_0/\rho_1 = 1.1$, and $\rho_0/\rho_2 = 2.9$, while for the right panel $c_0 \approx 105$, $c_1 = 100$, $c_2 \approx 111$, $v_{A0} = 1.0$, $v_{A1} = 0.5$, $v_{A2} = 0.7$, $\rho_0/\rho_1 = 1.1$, and $\rho_0/\rho_2 = 0.9$ were used.

distinct phase speeds as kx_0 increases. This limit of phase speed is influenced by the measure of density asymmetry R , and the relative magnitude of the Alfvén speeds. The difference in phase speed behavior apparent in Figures 5 and 6 may serve some practical interest. For instance, kink oscillations in the long-wavelength limit of a linear approximation of coronal loop description show nearly incompressible properties (Wang & Solanki 2004; Carter & Erdélyi 2007). Figure 6 thus contrasts wave dispersion in a rarefied medium to propagation in a dense, fat coronal loop, for which Figure 5 provides an approximation.

When the external densities are identical, the smaller the Alfvén speed difference is, the closer the dispersion solutions (i.e., phase speeds) approach one another as $kx_0 \rightarrow \infty$. In this case, the magnitude of R serves to determine what this common value exactly is; a lower R parameter takes the common value farther away from the internal Alfvén speed. Similarly, if the external Alfvén speeds are chosen to be identical, then the changes in R first drive the phase speed curves toward ever closer approaches in the $kx_0 \rightarrow \infty$ limit. Then the two solutions grow farther apart from one another again as R changes further.

3.2. Application to MBPs

A manifestation of an incompressible asymmetric magnetic slab may be found in MBPs of the solar photosphere. Found in the dark intergranular lanes formed from convective downflow, MBPs are small concentrations of intense magnetic field with strength of the order of kilogauss. They owe their brightness, on the one hand, to their lower plasma pressure, which allows observers to glance deeper into the photosphere, and on the other hand, to heating of the internal material by the environment (Roupe van der Voort et al. 2005; Crockett et al. 2010; Keys et al. 2013). MBPs are often treated as cylindrical flux tubes, although in reality they often possess strongly elongated or irregular shapes, especially near pores (Berger et al. 1995; Bovelet & Wiehr 2003). This opens up the possibility to treat an MBP locally as a magnetic slab. Furthermore, under the effect of neighboring granular cells, conditions on either side of an MBP may be different from one

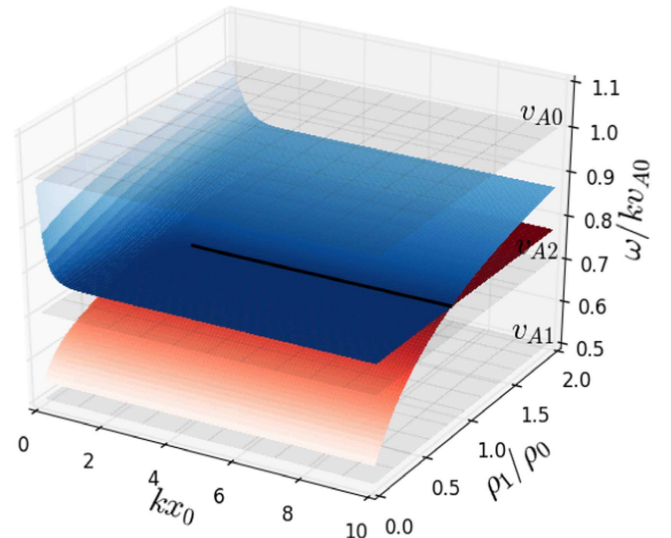


Figure 5. Slow surface mode solutions of Equation (34) in the incompressible limit, showing the dependence of the common limit of phase speeds on the density ratio ρ_1/ρ_0 . Blue indicates the quasi-sausage mode, while red applies to the quasi-kink mode. Here, $c_1 = 100.0$, $v_{A0} = 1.0$, $v_{A1} = 0.5$, and $v_{A2} = 0.7$ were used, while c_0 and c_2 were continuously changing in order to sustain total pressure balance between the domains. The black line indicates the values of the density ratio and the dimensionless slab width, for which the phase speeds of the quasi-sausage and quasi-kink modes perform a close approach and avoided crossing.

another. This, in turn, means that we can apply the magnetically asymmetric slab model to MBPs and their environment (as shown in Figure 7).

In order for the slab approach to be appropriate for describing an MBP, further considerations are needed. The configuration we have investigated is infinite in the y and z directions, whereas an actual bright point is a finite structure. It may, however, still be viewed as an unbounded slab if its dimensions are significantly greater than the wavelength of the modes examined.

There have been various studies that estimate the size of MBPs. Measuring with the Swedish Vacuum Solar Telescope on La Palma, Berger et al. (1995) found a lognormal size

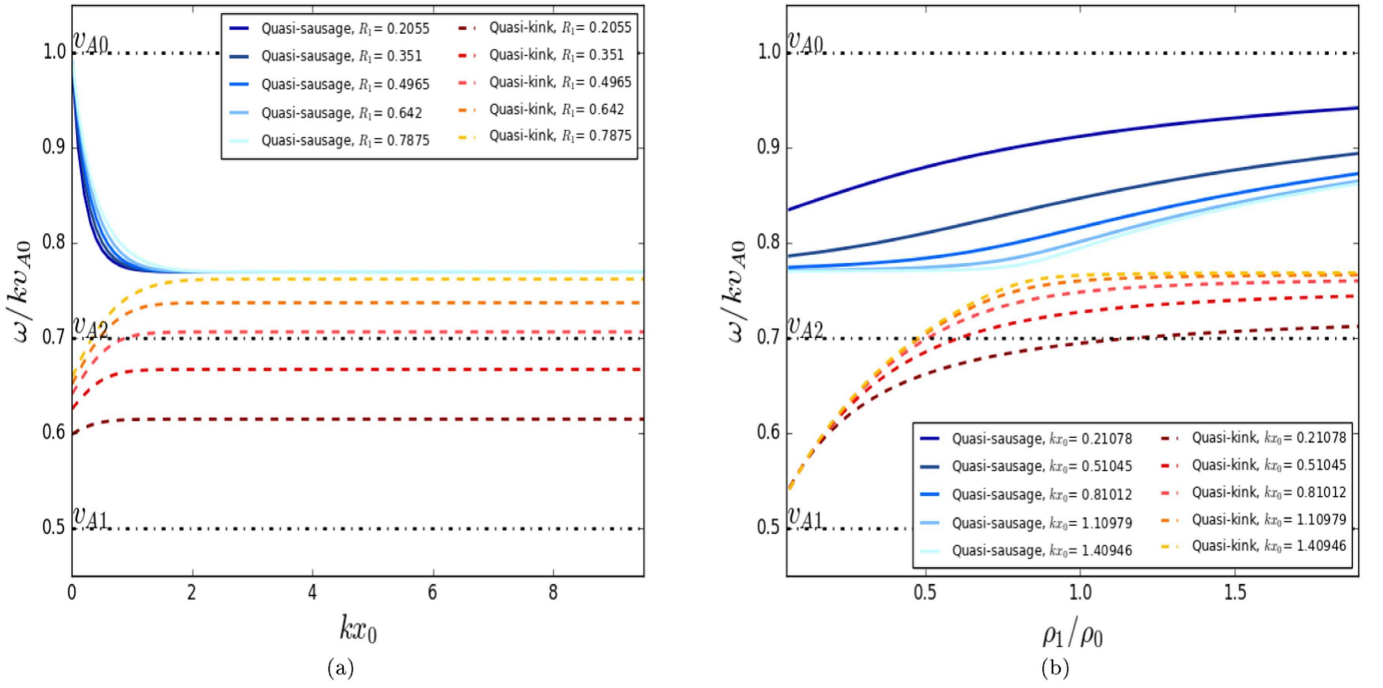


Figure 6. 2D projections of Figure 5, illustrating the effects of varying the equilibrium (a) slab width, kx_0 , and (b) density ratio ($R_1 = \rho_0/\rho_1$) on the incompressible eigenmodes of an asymmetric magnetic slab. Solid (dashed) lines represent quasi-sausage (quasi-kink) modes, and color coding indicates which pair of solutions is valid for which value of the equilibrium parameters.

distribution of MBPs with a modal value of 220 km ($0''.30$) and an average of 250 km ($0''.35$). Detecting MBPs with the Dutch Open Telescope, a similar result (dominant diameter of 220 ± 25 km) was obtained by Bovelet & Wiehr (2003), who also noted that only in about 2/3 of cases, isolated MBPs have circular shapes. Repeated observations—thanks to the higher resolution of the 1 m Swedish Solar Telescope (SST)—yielded somewhat lower dominant diameter values of 160 ± 20 km (Wiehr et al. 2004; Crockett et al. 2010). The analysis performed by Sánchez Almeida et al. (2004), with the help of two-Gaussian fits to MBPs on images taken by the SST, found major axis lengths of up to 350 km, while minor axis sizes peaked around 135 km (reaching the spatial resolution of the observations) and mostly stayed below 200 km. Solanki et al. (2010) concluded that the size of MBPs may be close to the $0''.15$ spatial resolution limit of the SUNRISE balloon-borne solar observatory (≈ 60 – 100 km). The lower limit on the size of MBPs seems to lie at a 100-km diameter, where radiative pressure stops the convective collapse of the tube (Venkatakrishnan 1986), or if interaction with acoustic waves keeps splitting the larger flux tubes, then somewhere between 40 and 60 km, according to Ryutova (1996).

Treating an MBP as a slab requires that its finite major axis should be much longer than the wavelengths of supported modes. Let us look at an elongated MBP with $x_0 = 1000$ km length (major axis) in the x dimension. If we suppose the waves should be able to complete at least 10 periods of oscillation, then the maximal wavelength that may be allowed is $\lambda = 100$ km (and so the wavenumber is $k = 2\pi \cdot 10^{-1} \text{ km}^{-1}$). The characteristic speeds in the photosphere are $c_s \approx 10 \text{ km s}^{-1}$ for the sound speed and $v_A \approx 8.25 \text{ km s}^{-1}$ for the Alfvén speed (Velli & Liewer 1999; Mullan 2009). As these values determine the phase speed of the waves, and we have just given an estimate of the angular wavenumber, it follows that the frequency of waves we might examine in a slab configuration is around

$\omega = 2\pi \cdot [0.0825, 0.1] \text{ Hz}$. Substituting these values (ω , v_{A0} , c_0) into the dispersion relation for the incompressible limit (Equation (23)) for a chosen slab width (x_0) leads to a relationship that binds together the internal and external densities, as well as the Alfvén speeds. Or if the magnetic field strength outside the slab is considered negligible, and the simpler asymmetric model detailed in Allcock & Erdélyi (2017) is taken to describe the MBP and its environment, then by using their Equation (27), we arrive at a relationship solely between the internal and external densities.

Depending on the wavelengths considered, an MBP as a magnetic slab may be approximated as either thin or wide. Using the estimation of $\lambda \approx 100$ km and considering that the width ($2x_0$) of an MBP may be only a few hundred kilometers, it turns out $kx_0 \ll 1$, so the MBP can be considered a thin slab for these waves. Then, the substitution $\tanh(kx_0) \approx kx_0$ can be made in the dispersion relation (34), and the angular frequency of possible modes is given as

$$\omega^2 = \frac{k^2}{2} \frac{1}{\rho_0(\rho_1^{-1} + \rho_2^{-1}) + 2\rho_0^2\rho_1^{-1}\rho_2^{-1} + 2} \times \{v_{A0}^2\rho_0(\rho_1^{-1} + \rho_2^{-1})K + 4v_{A0}^2\rho_0^2\rho_1^{-1}\rho_2^{-1} + R_E K + 2[v_{A1}^2 + v_{A2}^2] \pm [(v_{A0}^2\rho_0(\rho_1^{-1} + \rho_2^{-1})K - KR_E)^2 + 2v_{A0}^2(\rho_0^2\rho_1^{-1}\rho_2^{-1}KR_E - 4R_E K - 8\rho_0^2\rho_1^{-1}\rho_2^{-1}v_{A0}^2) + (4 + 4v_{A0}^2 + 4R_E K + 8\rho_0^2\rho_1^{-1}\rho_2^{-1}v_{A0}^2)(v_{A1}^2 + v_{A2}^2)]^{1/2}\}, \quad (38)$$

with the notation

$$R_E = \frac{\rho_0}{\rho_1} v_{A2}^2 + \frac{\rho_0}{\rho_2} v_{A1}^2, \quad (39)$$

$$K = kx_0 + \frac{1}{kx_0}. \quad (40)$$

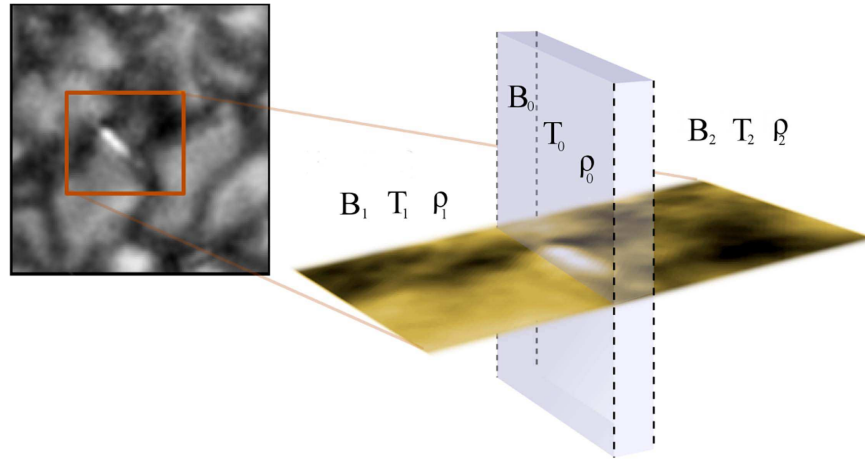


Figure 7. An elongated MBP is considered as an asymmetric magnetic slab configuration. The sketch is based on Figure 11 of Liu et al. (2018), showing TiO 7058 Å observations taken by the New Vacuum Solar Telescope.

If on the other hand we move toward larger wavenumbers (which might be even more difficult to detect), the MBP could be considered a wide slab ($1 \ll kx_0$), and using the approximation $\tanh(kx_0) \approx 1$, then Equation (34) can be reduced to give

$$\omega^2 = \frac{k^2}{2} \frac{1}{\rho_0(\rho_1^{-1} + \rho_2^{-1}) + \rho_0^2 \rho_1^{-1} \rho_2^{-1} + 1} \times \{v_{A0}^2 \rho_0(\rho_1^{-1} + \rho_2^{-1}) + 2v_{A0}^2 \rho_0^2 \rho_1^{-1} \rho_2^{-1} + R_E + [v_{A1}^2 + v_{A2}^2] \pm [(v_{A0}^2 \rho_0(\rho_1^{-1} + \rho_2^{-1}) - R_E)^2 + (1 + v_{A0}^2 + 2R_E + 2\rho_0^2 \rho_1^{-1} \rho_2^{-1} v_{A0}^2)(v_{A1}^2 + v_{A2}^2)]^{1/2}\}. \quad (41)$$

The estimated frequencies of the order of 0.1 Hz, however, still exceed the frequency of oscillations that our current instruments are able to observe routinely. The nonmagnetic equivalent of this problem is the issue of high-frequency acoustic waves, which could play an important role in chromospheric heating. They are readily excited by convective motions, but difficult to observe in practice due to the smearing effect of seeing (in ground-based observations) and the weakening of the signal by the width of the response function (in both space- and ground-based observations; see e.g., Fossum & Carlsson 2004, 2005). There are opposing views as to the power found in high-frequency oscillations. Based on the analysis of *TRACE* and later *Hinode* data, Fossum & Carlsson (2004, 2005), as well as Carlsson et al. (2007), deduced that for the most part, waves of frequency 5–40 mHz are responsible for carrying energy flux into the chromosphere; however, they seem to be unable to balance radiative losses. These results have been subject to criticism, as 2D and 3D hydrodynamic simulations generated a greater acoustic energy flux than was expected by Fossum & Carlsson (2005). It has also been pointed out that a direct comparison of theoretical models with *TRACE* observations requires caution; on length scales shorter than the limited spatial resolution of the instrument, small pockets of hotter material can be embedded in a relatively cold environment (Cuntz et al. 2007; Wedemeyer-Böhm et al. 2007).

Similarly, in order to unquestionably detect and identify waves in MBPs, extremely high spatial and temporal resolution is needed. For waves of 0.1 Hz, as given in the example above, consecutive samples ideally should be taken within five seconds, while still showing details of the order of a few tens of kilometers. Although currently we do not have measurements with the necessary resolution, once completed, the Daniel K. Inouye Solar Telescope (DKIST) will be able to meet these observational requirements. The construction of the 4 m Gregorian telescope in Haleakala, Maui, Hawaii, is soon coming to an end (it is predicted to be done in 2019, as of this writing), and then it will be utilized as the largest solar ground-based resource to study the dynamic magnetic activity of the Sun (Rimmele & ATST Team 2008; Berukoff et al. 2015). The DKIST Visible Broadband Imager (VBI) will operate with frame rates ≤ 30 Hz (which is already sufficient to identify our example wave), while working with the telescope’s $\approx 0''.03$ resolution (19 km on the Sun) (Tritschler et al. 2015), and so the instrument would be perfect to study possible wave phenomena in MBPs.

3.3. Parametric Solutions for the General Case

When the condition of incompressibility is not imposed, the dispersion relation (Equation (16)) has several more solutions. The existence of each eigenmode is determined by the ordering of internal and external characteristic speeds and the ratios of the external densities to the internal density.

Figure 8(a) illustrates the eigenmodes of the asymmetric magnetic slab when all of the sound speeds are higher than the corresponding Alfvén speeds in the three regions, and therefore $\beta > 1$ across the whole domain. In this case, with phase speeds (v_{ph}) smaller than the internal tube speed (c_{T0}), a pair of slow surface mode solutions exist. There are two bands of body modes, each of them containing an infinite number of harmonics (on the figure, only one pair of them is depicted for visibility). Slow body modes exist with $c_{T0} < v_{ph} < v_{A0}$, and fast body modes exist with $c_0 < v_{ph} < \min(c_1, c_2)$. This would be particularly important in applications when the two environments sandwiching the slab have different temperatures, e.g., waves propagating in the plume–interplume region. The cutoff occurs because it is prescribed that the waves should be evanescent as one moves farther from the slab. In the shaded

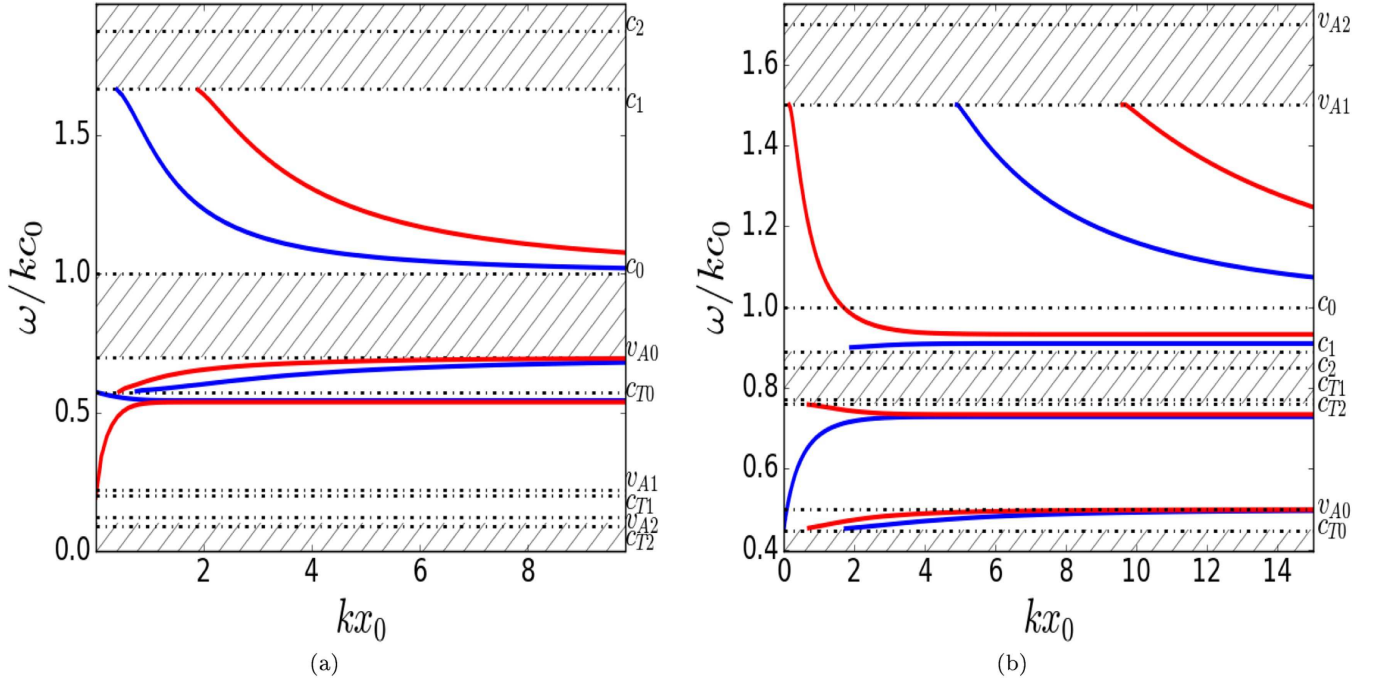


Figure 8. Dispersion diagrams for the dispersion relation (Equation (16)). Quasi-sausage (quasi-kink) modes are plotted in blue (red). (a) Slow and fast body modes, as well as slow surface mode waves, can exist if the Alfvén speed of each domain is smaller than the corresponding sound speed. The characteristic speed ordering is $v_{A0} = 0.7c_0$, $v_{A1} = 0.2c_0$, $v_{A2} = 0.1c_0$, $c_1 \approx 1.7c_0$, $c_2 \approx 1.9c_0$, $\rho_1/\rho_0 = 0.5$, and $\rho_2/\rho_0 = 0.4$. (b) Both fast and slow surface and body modes occur if the internal Alfvén speed is smaller than the internal sound speed, but the external Alfvén speeds are both higher than the corresponding sound speeds. The characteristic speed ordering is $v_{A0} = 0.5c_0$, $v_{A1} = 1.5c_0$, $v_{A2} = 1.7c_0$, $c_1 = 0.9c_0$, $c_2 = 0.85c_0$, $\rho_1/\rho_0 = 0.45$, and $\rho_2/\rho_0 = 0.39$.

regions of the figure, this condition is not met, and the waves become leaky.

In Figure 8(b), the internal Alfvén speed is still lower than the internal sound speed, but the external Alfvén speeds are greater than the corresponding sound speeds. In addition to the slow surface modes and the fast and slow body modes, this also gives existence to fast surface modes. The fast surface mode exists as a surface mode for the values of kx_0 below a cutoff, after which it changes character into an order one body mode. The fast surface quasi-sausage mode has a cutoff at the faster external sound speed value (with a phase speed below that, the wave would become leaky).

4. A Mechanical Analogy and Quasi-symmetric Oscillations

To facilitate the understanding of wave behavior in the magnetically asymmetric system, it is possible to expand upon the mechanical analogy introduced by Allcock & Erdélyi (2017). The asymmetric system presented in the present work, too, can be thought of as a coupled mechanical simple harmonic oscillation system, where the springs represent the three domains of plasma, and the small, massless plates correspond to the interfaces. While the central domain can still be represented with one spring, the two domains on the sides are each analogous to a pair of springs coupled in parallel. On Figure 9, blue springs represent the forces related to the external magnetic fields, and red springs represent kinetic restoring forces. The effective spring constant on either side will be the sum of the blue and red spring’s constant in this representation. If the spring constants k_{e1} and k_{e2} are equal on both sides, then we have the analog of the symmetric case examined by Edwin & Roberts (1982), as depicted in Figures 9(a)–(c).

If the spring constants of the magnetism- and density-related springs differ on each side (Figure 9(d)), then the eigenmodes of the system are analogous to the quasi-kink and quasi-sausage modes in a magnetic slab embedded in a magnetized plasma environment. If the oscillations of each plate are in-phase, then the motions correspond to the quasi-kink mode (Figure 9(e)), while oscillations in anti-phase are analogous to the quasi-sausage mode (Figure 9(f)).

Because of the existence of the external magnetic fields in the fully asymmetric slab model, it is possible to have different spring constants (equivalently, different magnetic field strengths and kinetic forces) on each side, but still reproduce an equilibrium that appears symmetric (Figure 9(g)). The condition for this is that the equivalent spring constants should be the same, that is $k_{11} + k_{12} = k_{22} + k_{21}$. When this is the case, the in-phase oscillations mimic the symmetric kink mode (Figure 9(h)), while the anti-phase oscillations correspond to the symmetric sausage mode (Figure 9(i)). Similarly, it is possible that an asymmetric magnetic slab will show oscillations that have similar qualities to the sausage and kink eigenmodes of a symmetric slab. First, we define “quasi-symmetric” modes to be eigenmodes that have equal transverse displacement amplitude on each boundary of the slab. This is equivalent to setting $\hat{v}_x(-x_0) = -\hat{v}_x(x_0)$ for quasi-sausage modes and $\hat{v}_x(-x_0) = \hat{v}_x(x_0)$ for quasi-kink modes. In general, these quasi-symmetric modes are distinct from symmetric modes because they can have different perturbation penetration depth in the external medium on each side of the slab and different spatial distribution of wave power within the slab.

An analytical relation can be given, which enables us to find a set of asymmetric parameters that imitates a symmetric system. In order to do this, we should consider that the structures of the symmetric and decoupled asymmetric

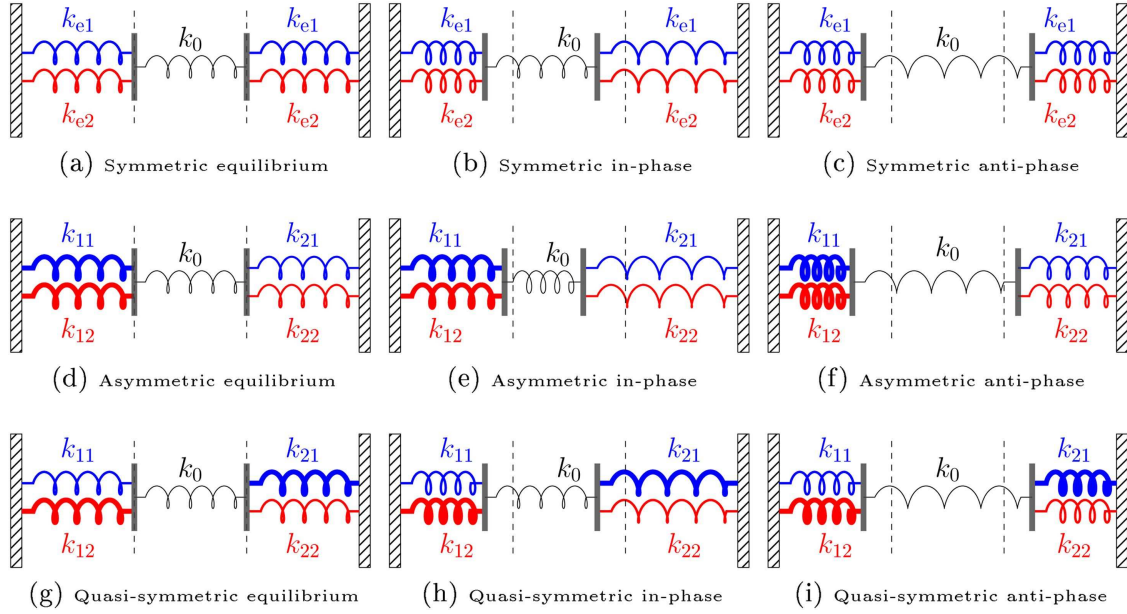


Figure 9. Externally asymmetric slab system as an analog to a coupled mechanical oscillator. Thicker springs correspond to higher spring constants k_{ij} . Panels (a), (d), and (g) show the symmetric, asymmetric, and quasi-symmetric spring systems in equilibrium. Panels (b) and (c) show the normal modes of a symmetric system. Panels (e) and (f) show the normal modes of an asymmetric system, while panels (h) and (i) depict the quasi-symmetric system. In each panel, the vertical dashed lines give the positions of the gray plates at equilibrium.

dispersion relations have to be the same:

$$\frac{\rho_0}{\rho_e} \frac{m_e}{(k^2 v_{Ae}^2 - \omega^2)} = -\frac{m_0}{(k^2 v_{A0}^2 - \omega^2)} \left(\frac{\tanh}{\coth} \right) \{m_0 x_0\},$$

$$\frac{1}{2} \left[\frac{\rho_0}{\rho_1} \frac{m_1}{(k^2 v_{A1}^2 - \omega^2)} + \frac{\rho_0}{\rho_2} \frac{m_2}{(k^2 v_{A2}^2 - \omega^2)} \right]$$

$$= -\frac{m_0}{(k^2 v_{A0}^2 - \omega^2)} \left(\frac{\tanh}{\coth} \right) \{m_0 x_0\}. \quad (42)$$

Here, quantities with index e refer to the symmetric system that the appropriate choice of asymmetric parameters is equivalent to. Since the right-hand sides in the two equations of Equation (42) are equal, the left-hand sides should also be the same:

$$\frac{\rho_0}{\rho_e} \frac{m_e}{(k^2 v_{Ae}^2 - \omega^2)}$$

$$= \frac{1}{2} \left[\frac{\rho_0}{\rho_1} \frac{m_1}{(k^2 v_{A1}^2 - \omega^2)} + \frac{\rho_0}{\rho_2} \frac{m_2}{(k^2 v_{A2}^2 - \omega^2)} \right]. \quad (43)$$

To ensure this relationship is met, we require that the two terms on the right to be equal:

$$\frac{\rho_0}{\rho_1} \frac{m_1}{(k^2 v_{A1}^2 - \omega^2)} = \frac{\rho_0}{\rho_2} \frac{m_2}{(k^2 v_{A2}^2 - \omega^2)} \quad (44)$$

Applying the definition we gave for quasi-symmetric modes, we will now show that Equation (44) is the necessary and sufficient condition on the magnetic and plasma parameters in the external regions that result in quasi-symmetric eigenmodes of an asymmetric magnetic slab for a given angular frequency ω and angular wavenumber k . To show that Equation (44) is a necessary condition, consider an asymmetric magnetic slab that supports quasi-symmetric modes. The transverse velocity perturbation solution is given by Equation (12), where the

coefficients may be expressed as

$$A = \frac{1}{C_1 - S_1} (BC_0 - CS_0), \quad (45)$$

$$D = \frac{1}{C_2 - S_2} (BC_0 + CS_0), \quad (46)$$

$$B = \frac{\Lambda_0 C_0 + \Lambda_1 S_0}{\Lambda_0 S_0 + \Lambda_1 C_0} C = -\frac{\Lambda_0 C_0 + \Lambda_2 S_0}{\Lambda_0 S_0 + \Lambda_2 C_0} C, \quad (47)$$

$$C \text{ is arbitrary}, \quad (48)$$

for quasi-sausage modes, and

$$A = \frac{1}{C_1 - S_1} (BC_0 - CS_0), \quad (49)$$

$$D = \frac{1}{C_2 - S_2} (BC_0 + CS_0), \quad (50)$$

$$C = \frac{\Lambda_0 S_0 + \Lambda_1 C_0}{\Lambda_0 C_0 + \Lambda_1 S_0} B = -\frac{\Lambda_0 S_0 + \Lambda_2 C_0}{\Lambda_0 C_0 + \Lambda_2 S_0} B, \quad (51)$$

$$B \text{ is arbitrary}, \quad (52)$$

for quasi-kink modes. For more detail on the derivation of these coefficients for a slab in a nonmagnetic asymmetric environment, see Allcock & Erdélyi (2018).

Given the supposition that the slab supports quasi-symmetric modes, we have, for quasi-sausage modes,

$$\hat{v}_x(-x_0) = -\hat{v}_x(x_0), \quad (53)$$

$$\Rightarrow \left(\frac{\Lambda_0 C_0 + \Lambda_1 S_0}{\Lambda_0 S_0 + \Lambda_1 C_0} \right) C_0 - S_0 = -\left(\frac{\Lambda_0 C_0 + \Lambda_1 S_0}{\Lambda_0 S_0 + \Lambda_1 C_0} \right) C_0 - S_0, \quad (54)$$

$$\Rightarrow \Lambda_0 C_0 + \Lambda_1 S_0 = 0. \quad (55)$$

Similarly, taking the second expression for B , we deduce that

$$\Lambda_0 C_0 + \Lambda_2 S_0 = 0, \quad (56)$$

therefore $\Lambda_1 = \Lambda_2$, which is equivalent to Equation (44). This concludes the proof that Equation (44) is a necessary condition for the existence of quasi-symmetric oscillations for quasi-sausage modes. For quasi-kink modes, a similar proof can be followed to show that $\hat{v}_x(x_0) = \hat{v}_x(-x_0)$ implies Equation (44).

To show that Equation (44) is a sufficient condition, consider an asymmetric magnetic slab with parameters that satisfy this formula. Under this supposition, the transverse velocity perturbation solution for quasi-sausage modes reduces to

$$\hat{v}_x(x) = \begin{cases} A(\cosh m_1 x + \sinh m_1 x) & \text{if } x < -x_0, \\ C \sinh m_0 x & \text{if } |x| \leq x_0, \\ D(\cosh m_2 x - \sinh m_2 x) & \text{if } x > x_0, \end{cases} \quad (57)$$

where

$$A = \frac{-CS_0}{C_1 - S_1}, \quad D = \frac{CS_0}{C_2 - S_2}, \quad C \text{ is arbitrary.} \quad (58)$$

Now, the solution within the slab, $|x| \leq x_0$, is an odd function of x , that is $\hat{v}_x(-x_0) = -\hat{v}_x(x_0)$. This concludes the proof that Equation (44) is a sufficient condition for the existence of quasi-symmetric oscillations in the case of quasi-sausage modes. For quasi-kink modes, a similar proof is followed, where we find that $\hat{v}_x(x) = B \cosh(m_0 x)$ is an even function within the slab. Therefore, Equation (44) is a necessary and sufficient condition for the existence of quasi-symmetric modes in a magnetic slab.

If we further specify that the penetration depths of perturbations in the external plasma are equal on each side of the slab, so that the eigenfunction is fully symmetric, then this implies that the external parameters are equal, and we have a symmetric slab. That is, a mode with a fully symmetric eigenfunction can exist only in a symmetric slab.

For an asymmetric slab, the condition (44) for quasi-symmetric oscillations creates a connection between the external parameters on the two sides of the slab, which, using Equation (3), can be restated as

$$\frac{(k^2 v_{A2}^2 - \omega^2) m_1}{(k^2 v_{A1}^2 - \omega^2) m_2} = \frac{\rho_1}{\rho_2} = \frac{c_2^2 + \frac{1}{2} v_{A2}^2}{c_1^2 + \frac{1}{2} v_{A1}^2}. \quad (59)$$

Thus, to find quasi-symmetric oscillations with a given angular frequency and wavenumber, one of the external characteristic speeds can be determined as a function of the other three. This, of course, means that (substituting for the expressions of characteristic speeds) one unknown external magnetic field strength, density, or pressure (or temperature) can also be determined as a function of the other five such quantities, so that the slab will produce seemingly symmetric oscillations.

5. Discussion

Both theoretical and observational studies of MHD waves have entered a golden age. Two main factors drive this research: the prospect of understanding atmospheric heating, and the possible magneto-seismological application. By developing theoretical models, with the help of dispersion relations describing certain simple configurations, it is possible to find the connection between characteristics of a wave and those of the medium guiding it.

Sometimes it is difficult or impossible to measure certain physical parameters (such as heat transport coefficients or

magnetic field strengths) of a given phenomenon in the solar atmosphere. Measurements of wave properties (e.g., the wavelength or period) in solar structures and a comparison with the results expected from theoretical models allow us to draw conclusions about unknown background quantities of the waveguide (Verth et al. 2007; Verth & Erdélyi 2008; Andries et al. 2009; Ruderman & Erdélyi 2009; Morton et al. 2012). Nowadays, the amount and resolution of data from space- and ground-based instruments offer us a unique possibility for SMS applications; therefore, it is even more useful to improve our understanding of MHD wave propagation in simple configurations (see e.g., Erdélyi 2006a, 2006b).

In this spirit, as a further important generalization of the symmetric slab model described by Edwin and Roberts (Roberts 1981a, 1981b; Edwin & Roberts 1982), the mathematical model of a magnetic slab in an asymmetric magnetic environment has been introduced in the current paper. Previous work on the slab in an asymmetric, but field-free environment, by Allcock & Erdélyi (2017) showed that there are fundamental differences between slabs with symmetric or asymmetric surroundings. These results have been corroborated and expanded upon by the current study. Our main findings are the following:

1. The derivation of the dispersion relation for a magnetic slab, which is embedded in an asymmetric magnetized environment. The principal distinction is that for the asymmetric slab (regardless of the magnetic field strength of the environment), the dispersion relation does not decouple into two equations. This implies that the eigenmodes of a slab in an asymmetric environment are not the traditionally known decoupled sausage and kink modes, but are rather waveforms with mixed properties, referred to as quasi-sausage and quasi-kink modes.
2. Wave behavior may, however, approximate the usual modes, but only when the external equilibrium parameters describing the magnetized plasma on either side of the slab are of the same order. The decoupled form of the dispersion relation is reminiscent of the one describing the symmetric slab model, and has “sausage” and “kink” mode solutions, which are affected by the presence of the different external plasma densities and field strengths. For example, the asymmetric quasi-sausage mode leaves a surface other than that at the center of the slab unperturbed, and the asymmetric quasi-kink mode does not necessarily preserve the volume of the slab.
3. Analytical solutions of the dispersion relation have been presented and complemented by parametric examination. It appears that all the well-known modes (surface, body, quasi-sausage, quasi-kink, fast, and slow) may appear in a weakly asymmetric configuration as well and in many cases with changed properties (such as cut-off frequencies).
4. For an asymmetric slab in a nonmagnetic environment, this model has the potential to serve as a diagnostic tool in SMS. It has been discussed that, due to the discrepancy between external parameters, the same perturbation will not have the exact same effect on the two sides of the slab. The ratio of the oscillation amplitudes on either boundary of the slab will naturally depend on the internal and external physical parameters of the model. This ratio is an observable quantity, so if it can be determined as a function of the slab parameters, then these parameters

may be deduced from observations of the cross-slab amplitude ratio (and other characteristics of the system such as the frequency of the waves or the width of the slab).

Although solar magnetic structures are frequently modeled in cylindrical geometry, there are regions where the Cartesian slab model can be well applied. We have shown one such possible application in the form of MBPs of the solar photosphere. These intense concentrations of magnetic flux often take elongated shapes, and they may therefore be more appropriately considered as magnetic slabs embedded in intergranular lanes between granules of distinct plasma parameters. In order to study such small-scale wave phenomena, extremely high spatial and temporal resolution is needed, such as those the DKIST will be able to provide.

The slab model is a simple, yet versatile, approach to the study of MHD waves. The precise nature of the supported modes in any waveguide will, however, depend upon the details of the geometry and the differences in internal and external physical parameters. Varying these characteristics, the asymmetric slab model can be adapted to describe a wide variety of phenomena, such as prominences or coronal loop boundaries. For this reason, we explore wave propagation in certain specific cases, including the thin and wide slab approximations and the low and high plasma beta limits, in a follow-up paper.

The authors acknowledge the support received from the Erasmus Programme of the EU for enabling this research. N.Z. is also grateful to Eötvös Loránd University, the University of Debrecen, and the University of Sheffield. M.A. acknowledges support from the University Prize Scholarship at the University of Sheffield. R.E. is grateful to Science and Technology Facilities Council (STFC) UK and the Royal Society (UK) for the support received.

ORCID iDs

Noémi Kinga Zsámberger  <https://orcid.org/0000-0002-2822-129X>

Matthew Allcock  <https://orcid.org/0000-0002-0771-743X>

Róbert Erdélyi  <https://orcid.org/0000-0003-3439-4127>

References

- Allcock, M., & Erdélyi, R. 2017, *SoPh*, **292**, 35
 Allcock, M., & Erdélyi, R. 2018, *ApJ*, submitted
 Andries, J., van Doorselaere, T., Roberts, B., et al. 2009, *SSRv*, **149**, 3
 Arregui, I. 2015, *RSPTA*, **373**, 20140261
 Arregui, I., Oliver, R., & Ballester, J. L. 2012, *LRSP*, **9**, 2
 Aschwanden, M. 2005, *Physics of the Solar Corona* (Berlin: Springer)
 Aschwanden, M. J., Fletcher, L., Schrijver, C. J., & Alexander, D. 1999, *ApJ*, **520**, 880
 Banerjee, D., Erdélyi, R., Oliver, R., & O'Shea, E. 2007, *SoPh*, **246**, 3
 Berger, T. E., Schrijver, C. J., Shine, R. A., et al. 1995, *ApJ*, **454**, 531
 Berukoff, S., Reardon, K., & Rimmele, T. 2015, in *ASP Conf. Ser. 495*, *Astronomical Data Analysis Software and Systems XXIV (ADASS XXIV)*, ed. A. R. Taylor & E. Rosolowsky (San Francisco, CA: ASP), 91
 Bovelet, B., & Wiehr, E. 2003, *A&A*, **412**, 249
 Carlsson, M., Hansteen, V. H., de Pontieu, B., et al. 2007, *PASJ*, **59**, S663
 Carter, B. K., & Erdélyi, R. 2007, *A&A*, **475**, 323
 Crockett, P. J., Mathioudakis, M., Jess, D. B., et al. 2010, *ApJL*, **722**, L188
 Cuntz, M., Rammacher, W., & Musielak, Z. E. 2007, *ApJL*, **657**, L57
 de Moortel, I. 2009, *SSRv*, **149**, 65
 De Moortel, I., & Browning, P. 2015, *RSPTA*, **373**, 20140269
 De Moortel, I., & Nakariakov, V. M. 2012, *RSPTA*, **370**, 3193
 De Pontieu, B., Erdélyi, R., & De Moortel, I. 2005, *ApJL*, **624**, L61
 Edwin, P. M., & Roberts, B. 1982, *SoPh*, **76**, 239
 Erdélyi, R. 2006a, *RSPTA*, **364**, 351
 Erdélyi, R. 2006b, in *Proc. SOHO 18/GONG 2006/HELAS I, Beyond the Spherical Sun*, ed. K. Fletcher & M. Thompson (ESA SP-624; Noordwijk: ESA), 15
 Fossum, A., & Carlsson, M. 2004, in *Proc. SOHO 13–Waves, Oscillations, and Small-Scale Transient Events in the Solar Atmosphere: A Joint View from SOHO and TRACE*, ed. H. Lacoste (ESA SP-547; Noordwijk: ESA), 125
 Fossum, A., & Carlsson, M. 2005, in *Astrophysics and Space Science Library 320, Solar Magnetic Phenomena*, ed. A. Hansmeier, A. Veronig, & M. Messerotti (Dordrecht: Springer), 239
 Goossens, M., Erdélyi, R., & Ruderman, M. S. 2011, *SSRv*, **158**, 289
 Habbal, S. R., Holzer, T. E., & Leer, E. 1979, *SoPh*, **64**, 287
 Keys, P. H., Mathioudakis, M., Jess, D. B., et al. 2013, *MNRAS*, **428**, 3220
 Komm, R., De Moortel, I., Fan, Y., Ilonidis, S., & Steiner, O. 2015, *SSRv*, **196**, 167
 Liu, Y., Xiang, Y., Erdélyi, R., et al. 2018, *ApJ*, submitted
 Mathioudakis, M., Jess, D. B., & Erdélyi, R. 2013, *SSRv*, **175**, 1
 Morton, R. J., Verth, G., McLaughlin, J. A., & Erdélyi, R. 2012, *ApJ*, **744**, 5
 Mullan, D. J. 2009, *Physics of the Sun: A First Course* (Boca Raton, FL: CRC Press)
 Rimmele, T. R. & ATST Team 2008, *AdSpr*, **42**, 78
 Roberts, B. 1981a, *SoPh*, **69**, 39
 Roberts, B. 1981b, *SoPh*, **69**, 27
 Roberts, B. 2000, *SoPh*, **193**, 139
 Roupe van der Voort, L. H. M., Hansteen, V. H., Carlsson, M., et al. 2005, *A&A*, **435**, 327
 Ruderman, M. S., & Erdélyi, R. 2009, *SSRv*, **149**, 199
 Ryutova, M. 1996, *ApL&C*, **34**, 71
 Sánchez Almeida, J., Márquez, I., Bonet, J. A., et al. 2004, *ApJL*, **609**, L91
 Solanki, S. K., Barthol, P., Danilovic, S., et al. 2010, *ApJL*, **723**, L127
 Tritschler, A., Rimmele, T. R., Berukoff, S., et al. 2015, in *18th Cambridge Workshop on Cool Stars, Stellar Systems, and the Sun 18*, ed. G. T. van Belle & H. C. Harris, 933
 Uchida, Y. 1968, *SoPh*, **4**, 30
 Velli, M., & Liewer, P. 1999, *SSRv*, **87**, 339
 Venkatakrishnan, P. 1986, *Natur*, **322**, 156
 Verth, G., & Erdélyi, R. 2008, *A&A*, **486**, 1015
 Verth, G., Van Doorselaere, T., Erdélyi, R., & Goossens, M. 2007, *A&A*, **475**, 341
 Wang, T. 2011, *SSRv*, **158**, 397
 Wang, T. J., & Solanki, S. K. 2004, *A&A*, **421**, L33
 Wedemeyer-Böhm, S., Steiner, O., Bruls, J., & Rammacher, W. 2007, in *ASP Conf. Ser. 368, The Physics of Chromospheric Plasmas*, ed. P. Heinzel, I. Dorotovič, & R. J. Rutten (San Francisco, CA: ASP), 93
 Wiehr, E., Bovelet, B., & Hirzberger, J. 2004, *A&A*, **422**, L63
 Zaqarashvili, T. V., & Erdélyi, R. 2009, *SSRv*, **149**, 355